

Multi-objective Optimization of Lighting System Design for Automatic Image Measurement and Inspection Machine

Jian-Long Kuo*

Department of Mechatronics Engineering,
National Kaohsiung University of Science and Technology, Kaohsiung 811, Taiwan

(Received December 6, 2021; accepted April 7, 2022)

Keywords: lighting system, automatic image measurement, image inspection machine, multi-objective optimization

A 3D automatic sensing measurement system was developed to improve image processing technology for inspecting electronic parts. The developed system can automatically and rapidly measure a small workpiece, such as the width and center position of a circular aperture, and the distance, length, and angle of a geometrical shape. Through the optimization of the light system design, the 3D automatic measurement system can maximize the efficiency of the measurement. This measurement system includes two parts. The first part is an optics servo system including a standardized system, a turret-type magnification, and a zoom lens. The second part is a photo source servo system including an objective table, coaxial light, four-split ring light, and colored photo source. Each measurement routine of the testing workpiece must be programmed in advance by using QVPAK software. QVPAK controls multiple sensors such as a vision sensor, touch probe, continuous scanning devices, and special ultra micro accurate probes (UMAPs) or long-range nano probes (LNPs). The moving position of the 3D platform of the system can be controlled. The developed program can be transformed into a Visual Basic program. The system can automatically measure a large processed workpiece. Two objective functions, measuring precision and measuring time, are selected to improve the design. The response surface method is combined with a multiple performance characteristic index for multi-objective optimization, which is carried out using orthogonal particle swarm optimization. This experiment confirmed the short measuring time of the system. Human error can be avoided when using this system, and the accuracy may reach up to 0.002 mm. The proposed multi-objective optimization technique for detecting workpieces of electronic parts can increase the image processing efficiency. The discussed algorithm can be uploaded onto a cloud server to provide a 3D automatic measurement system for sensing and inspecting the workpieces of electronic parts. Intelligent manufacturing via a cloud server can be achieved in the era of Industry 4.0.

*Corresponding author: e-mail: jlkuo@nkust.edu.tw
<https://doi.org/10.18494/SAM3807>

1. Introduction

1.1 Review of image sensors and inspection techniques

Inspection techniques for electronic packaging are required in highly automated generation processes. Conventional inspections are often performed manually by humans and are usually inefficient.

Recently, the size of electronic packaging has reached the nanometer range. A microscope is usually required to check for defects in electronic components. A human inspector might neglect a defect due to a lack of experience.

The conventional method of inspecting tiny objects is to use an inspection probe with contact measurement. However, the contact might damage the surface of the objects. Three-dimensional optical laser inspection is widely used as a noncontact measurement method to prevent the surface of a workpiece from damage. By image processing, the range of inspection is globally wide and rapid. Therefore, it is a popular technique in electronic packaging.

1.2 Review of 3D image measurement and inspection

Stout introduced some commonly used 3D measurement techniques.⁽¹⁾ Although profiling techniques have been widely used in industry and academic research for manufacturing control and functional control of surface roughness, in some cases, the profiling techniques and 2D parameters defined in standards are inadequate and/or unsuitable for characterizing surfaces. Hough reported various methods of identifying image patterns.⁽²⁾ These methods are particularly adaptable to the study of subatomic particle tracks passing through a visual field. Cao proposed automatic methods of micro-dimension measurement using image processing.⁽³⁾ In Cao's paper, a technique to measure the locations and orientations of apertures and their diameters on the spout nozzle of an engine was presented and a complex measuring apparatus designed for this purpose was discussed. Beckwith and Marangoni discussed various mechanical measurement methods to obtain 3D geometric sizes and surface properties.⁽⁴⁾ With an emphasis on precision and clarity, their book covered fundamental issues common to all areas of measurement, with individual chapters on applied areas of measurement.

Kawasue and Ishimatsu employed circular image shifting motion for the 3D measurement of moving objects,⁽⁵⁾ where a new approach to 3D measurement of the position and velocity of moving particles was introduced. Subbarao and Choi discussed the image recovery principle for 3D shapes for a target image.⁽⁶⁾ They described a new shape-from-focus method that was based on a new concept named the focused image surface. Pentland illustrated a new technique for sensing the depth of field.⁽⁷⁾ He examined a novel source of depth information: focal gradients resulting from the limited depth of field inherent in most optical systems. Nayar and Nakagawa proposed an effective approach to measure a rough surface.⁽⁸⁾ They also illustrated that suitable pattern analysis and machine intelligence can be used to analyze surface images.⁽⁹⁾ They presented two algorithms for depth estimation. The first algorithm simply looked for the focus level that maximizes the focus measure at each image point. The second algorithm used a Gaussian model to interpolate the focus measures to obtain more accurate depth estimates.

1.3 Description of analytic methodology

Lu and Antony discussed the use of fuzzy inference rules and multiple response surfaces to obtain optimal solutions.⁽¹⁰⁾ Their approach took advantage of both the Taguchi method and a fuzzy-rule based inference system, resulting in a robust and practical methodology in tackling multiple-response optimization problems. Tarng *et al.* proposed a fuzzy logic method to optimize the submerged arc welding process.⁽¹¹⁾ They used fuzzy logic in the Taguchi method to optimize the submerged arc welding process with multiple performance characteristics.

Tong *et al.* used principal component analysis to optimize multiple response surfaces⁽¹²⁾ and proposed a novel optimization procedure for multiple responses based on Taguchi's parameter design. Wu proposed the use of principal component analysis to derive a robust design for multiple quality characteristics,⁽¹³⁾ presenting an approach to optimizing multiple correlated quality characteristics based on the modified double-exponential desirability function. Myers and Douglas discussed a response surface method (RSM) for obtaining a statistical model for associated problems.⁽¹⁴⁾ They discussed many topics such as optimal designs, optimization techniques, robust parameter design, methods for design evaluation, computer-generated designs, multiple response optimization, and non-normal responses.

Using the RSM, Koyamada *et al.* selected the control factors in a studied problem and obtained the optimal parameters.⁽¹⁵⁾ They proposed a parameter optimization technique using the response surface methodology for accurate biological cell simulation. Parkinson formulated an engineering problem in an automatic manufacturing process⁽¹⁶⁾ and examined how engineering models can be used to develop robust designs.

Sundaresan *et al.* provided a procedure that incorporates manufacturing and operational variances to achieve designs with robust and optimal performance.⁽¹⁷⁾ They proposed a suitable optimization technique involving the definition of variables and constraints.

In this study, we designed a system that is suitable for finding the optimal parameters for sensing an image. We confirmed that the proposed system had a short measuring time. Human error can be avoided when using the system, and the accuracy can reach up to 0.002 mm. We demonstrated that the proposed multi-objective optimization technique for detecting workpieces of electronic parts can increase the image processing efficiency.

2. Optical Image Sensor and Automatic Inspection System

2.1 Image sensor and measurement system

It is not possible to measure tiny electronic components accurately using a conventional contact measuring technique. To overcome this problem, many advanced image processing techniques have been proposed.

An image processing technique includes three parts: pre-processing, post-processing, and noise reduction. Sometimes, when the image quality is poor, the automatic inspection machine shuts down during processing.

lens to the target area. The obtained images of objects are then transmitted to a PC for image processing and analysis.

2.2.1 Optical auxiliary system

The parts of an optical auxiliary system are listed in Table 1. The measurement precision depends on the quality of the image obtained using QVPAK software. QUICK VISION software is used to set up the different parameters for the lighting system.

2.2.2 Light source auxiliary system

A light source auxiliary system can be selected to provide the appropriate image effect. The types of light in the system are listed in Table 2. The effects of carrier light, coaxial light, and four-split ring light on an image are shown in Fig. 2.

Table 1
Optical auxiliary system.

| | |
|-----------------------------|--|
| Prime lens | Prime lens located at bottom of CCD. |
| Turret-type zoom lens | Three turret-type zoom lenses can rotate to change the zoom ratio. |
| Adjustable zoom object lens | Adjustable zoom object lens can be set to 15 positions. |

Table 2
Light source auxiliary system.

| | |
|-----------------------|---|
| Carrier light | Carrier light source located at bottom of workpiece. |
| Coaxial light | Light source passing through lens can increase contrast of object surface for z-axis measurement. |
| Fixed ring light | Fixed ring light located in area surrounding lens. |
| Four-split ring light | Programmable ring light (PRL) provided for further four-split ring light control to improve image effect. |
| Color lights | Four color lights selected: white, red, green, and blue. |

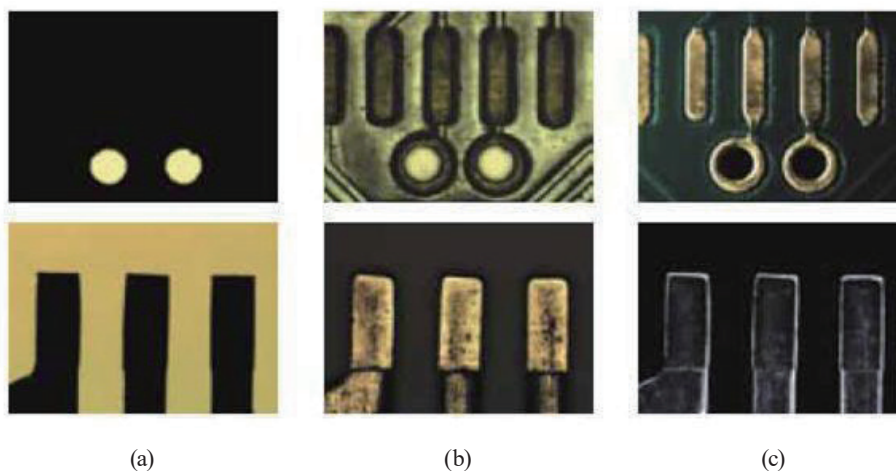


Fig. 2. (Color online) Effects of (a) carrier light, (b) coaxial light, and (c) four-split ring light on image.

2.2.3 Laser probe

As shown in Fig. 3, a laser probe is used to improve the surface measurement using z-axis position control. The laser probe can measure the ball grid array of surface-mount packaging and the C-type lead wire used in wire bonding.

2.2.4 Contact probe

As shown in Figs. 4 and 5, the contact probe is controlled by QUICK VISION software. The contact probe can measure the surface condition of the workpiece.

2.2.5 Rotational accessory

The rotational accessory is a bracket metal plate used to rotate the workpiece by any specific angle. QVPAK software can control the rotational angle with a resolution of up to 0.1° .

2.2.6 Joystick control box

A joystick control box, whose specifications are given in Table 3, is used to manually move the mask position in the z-direction.

2.2.7 Lighting system

In QVPAK, there are three types of light sources: coaxial light, carrier light, and ring light. For example, when inspecting the surface of an object, the surface gradient effect should be emphasized, and when inspecting the workpiece border, the border gradient should be sharpened.

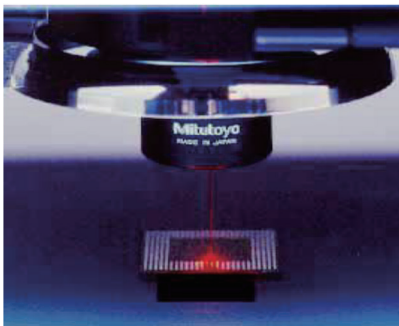


Fig. 3. (Color online) Laser probe.

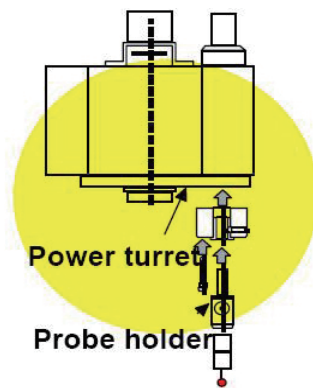


Fig. 4. (Color online) Schematic diagram of contact probe.



Fig. 5. (Color online) Image of contact probe.

Table 3
Joystick control box.

| Function | Description |
|----------------|--|
| Power | QUICK VISION power |
| Emergency | Emergency stop |
| Joystick | Control motion of carrier |
| Speed | CNC speed control |
| Status LED | Display status of machine |
| Measure | Control motion of probe |
| GOTO/interrupt | Interrupt routine for CNC mode and GOTO function for learning mode |
| TS key | ON/OFF of probe or laser |
| Cancel | Cancel function |

2.2.8 Light source system

The QVPAK light source system in the 3D inspection machine is shown in Fig. 6. The system includes carrier light, coaxial light, ring light, and optional four-split ring light.

2.3 Image sensor and measurement software

2.3.1 Brightness and contrast regulation

The brightness and contrast of the light sources in the system can be regulated independently.

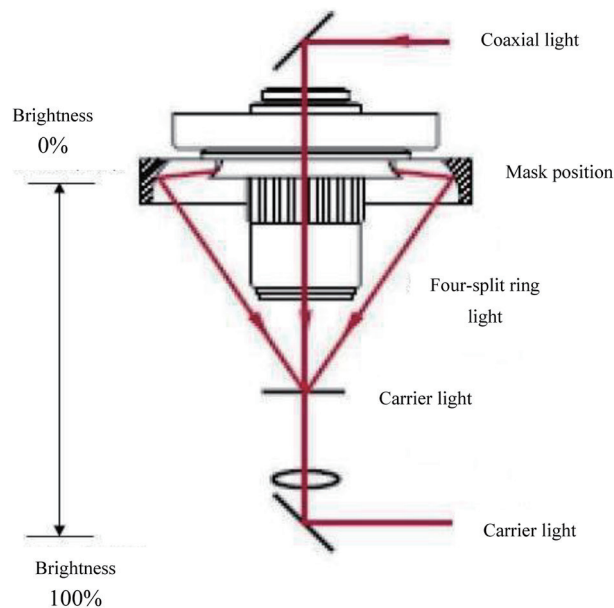


Fig. 6. (Color online) Lighting system in the 3D inspection machine.

2.3.2 Four-split ring light source

A four-split ring light source is a special hardware accessory. It can improve the image border of a slot border, tilt border, and transparent workpiece, and it can increase the gradient effect to emphasize the border of an object with the help of the reflection and shadow.

A PRL is divided into four quarter-circle parts: front, rear, right, and left parts, which can be set up separately. The light angle and tilt can also be regulated as shown in Figs. 7 and 8. Upon increasing the height of the PRL above the workpiece, the light sources irradiate the workpiece vertically, whereas the light sources irradiate the workpiece obliquely at a low height.

2.3.3 Color light source

The color light source can improve the contrast of the border of the object. To sharpen the border, the same background color is set. Reversely, if we want to soften the border, the inverted color is set.

2.3.4 Brightness tool

As shown in Fig. 9, the light source can regulate the optimal brightness of the target image. Two modes are included. In the independent mode, the four-split ring light moves to the appropriate light source position with a reset mode. In the dependent mode, the light source moves to the appropriate position directly without a reset mode.

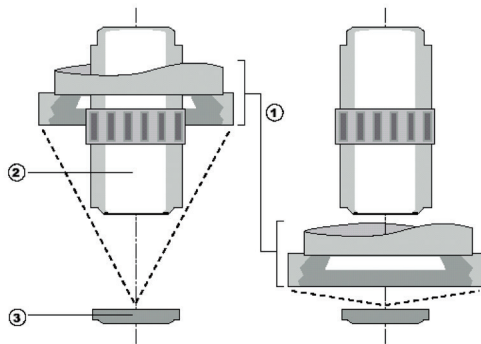


Fig. 7. Four-split ring light position at 30 and 80°.

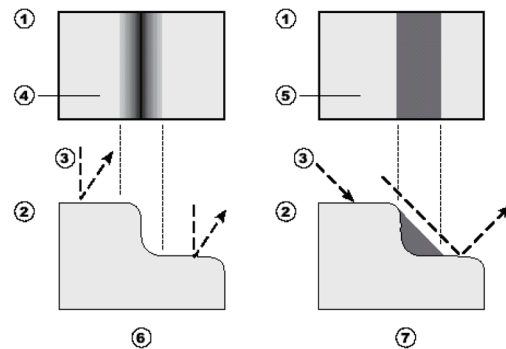


Fig. 8. Four-split ring light illuminating the tilt border.

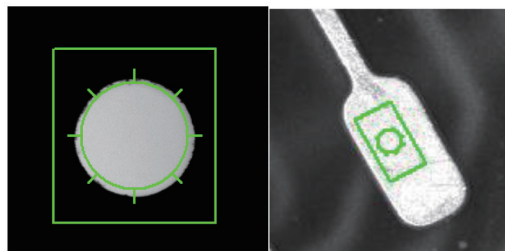


Fig. 9. (Color online) Image pattern obtained with brightness tools.

2.3.5 Dual-area contrast tool

As shown in Fig. 10, a dual-area contrast tool can improve the contrast of two areas of the target image and increase the measurement reliability. When the function is executed, the light source can provide the appropriate contrast of two areas of the target image.

2.3.6 Image processing and analyzing functions

As shown in Fig. 11, the image processing and analyzing functions are set up in an industrial PC. The automatic optical inspection system can perform the automatic processing for inspection using Visual Basic software.

3. Multi-objective Optimization by RSM

3.1 Control factors and level definition

Three control factors, the coaxial light, four-split ring light, and mask position, are selected to study the optimal precision and optimal time for image inspection by the RSM.

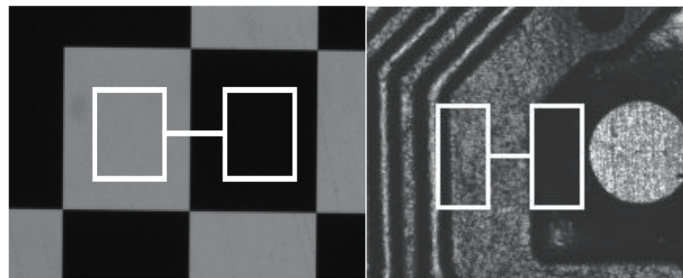


Fig. 10. (Color online) Image pattern obtained with dual-area contrast tool.



Fig. 11. (Color online) Image sensing machine and automatic inspection system.

The coaxial light and four-split ring light are both positive light sources. Because positive light sources have greater impact than the backlight sources, positive light sources are here selected as study targets.

The color light is also a key factor for workpieces of different colors. To simplify the measurement, a white light source is selected. In the RSM, nominal-the-best is selected to study the measuring precision. To transform the nominal-the-best problem into a larger-the-better problem, the following relation is used:

$$LTB_{value} = \frac{1}{Target_{value} - NTB_{value}}, \quad (1)$$

where LTB_{value} is the measurement for the larger-the-better problem, NTB_{value} is the measurement for the nominal-the-best problem, and $Target_{value}$ is the target value for the nominal-the-best problem.

On the other hand, smaller-the-better is selected to study the measuring time. To transform the smaller-the-better problem into the larger-the-better problem, the following relation is used:

$$LTB_{value} = \frac{1}{STB_{value}}, \quad (2)$$

where LTB_{value} is the measurement for the larger-the-better problem and STB_{value} is the measurement for the smaller-the-better problem.

Figure 12 shows the levels of the three control factors: factor A (coaxial light), factor B (four-split ring light), and factor C (mask position). The level definitions for the three control factors in the RSM are defined in Table 4.

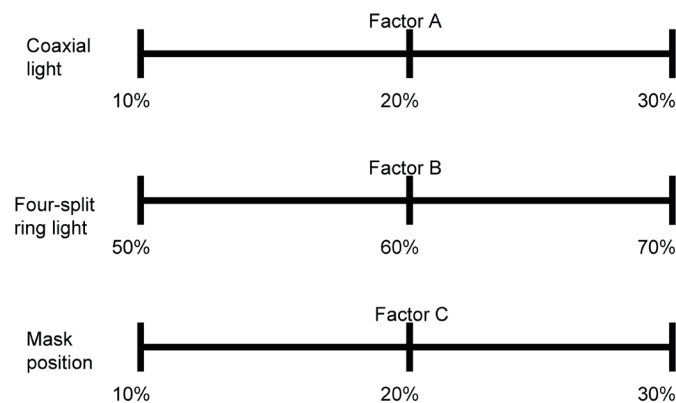


Fig. 12. Level definitions for factor A (coaxial light), factor B (four-split ring light), and factor C (mask position).

Table 4
Definitions of levels for the three control factors in the RSM.

| | Level 1 | Level 2 | Level 3 |
|------------------------------|---------|---------|---------|
| A: coaxial light (%) | 10 | 20 | 30 |
| B: four-split ring light (%) | 50 | 60 | 70 |
| C: mask position (%) | 10 | 20 | 30 |

3.2 Optimization cases

Three cases are studied to compare the optimization of the studied problem. The objective functions of Cases 1–3 are measuring precision and measuring time, respectively. The multiple objective functions of Case 3 are both measuring precision and measuring time. Because of the limited space, only Case 3 is discussed in detail, but similar mathematical processes apply to Cases 1 and 2.

In Case 3, a multiple performance characteristic index (MPCI) fuzzy-based dual RSM is used to formulate the multiple objective functions. Both the measuring precision and measuring time are considered together as one compact objective function to obtain the optimal solution. The first objective function is measuring precision. Nominal-the-best is used to obtain the optimal precision for the image inspection. The second objective function is measuring time. Smaller-the-better is used to obtain the minimal operation time for the image inspection. To unify the experimental data, the nominal-the-best problem is converted into a larger-the-better problem and the smaller-the-better problem is converted into a larger-the-better problem.

In the dual RSM, a combinational table including 16 experimental runs is used to perform experiments for different combinations of levels. In addition to the three control factors, two noise factors are also added to consider the possible variation in the experiments.

Two environmental lights that may interfere with the experimental measurements are considered as noise factors. The first light source is an LED light near the testing machine and the second light source is the fluorescent lamp in the testing room. For the three level definitions, color temperatures of 5000, 6000, and 7000 K are used to assess their effect on experiments. The lighting system of the testing machine and the fluorescent lamp of the testing room may slightly affect the target image.

Sixteen standard experimental runs are performed in the RSM. Four central-point experiments are also performed to study the central-point condition in the RSM. Cases 1–3 are studied to obtain the optimal values for the multiple objective functions.

3.3 Fuzzy inference and MPCI value

To integrate the two objective functions into one compact MPCI value, it is necessary to use a fuzzy inference process to obtain the MPCI value. In this process, the input membership function of the measuring precision is defined as shown in Fig. 13, where the triangular functions of fuzzy meanings S_1 , M_1 , and L_1 are defined. The input membership function of the measuring time is defined in Fig. 14, where the triangular functions of fuzzy meanings S_2 , M_2 , and L_2 are

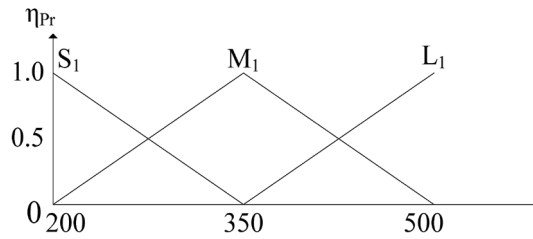


Fig. 13. Membership function of the S/N ratio of the measuring precision.

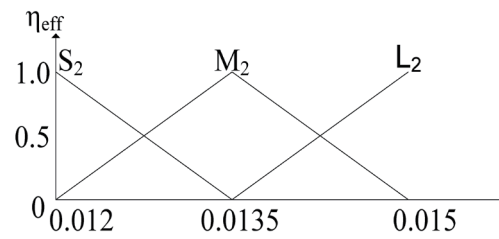


Fig. 14. Membership function of the S/N ratio of the measuring time.

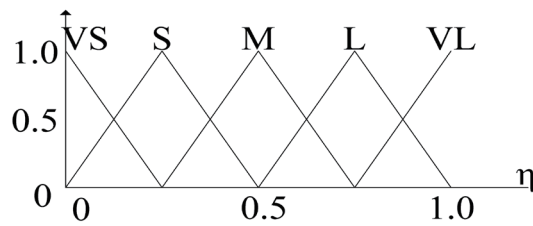


Fig. 15. Membership function of the MPCCI value.

Table 5
Fuzzy inference table.

| | | S/N ratio of time | | |
|------------------------|----------------|-------------------|----------------|----------------|
| | | S ₂ | M ₂ | L ₂ |
| S/N ratio of precision | S ₁ | VS | S | M |
| | M ₁ | S | M | L |
| | L ₁ | M | L | VL |

defined. The output membership function of the MPCCI value is defined in Fig. 15, where the triangular functions of fuzzy meanings VS, S, M, L, and VL are defined. The MPCCI value is normalized in the range of (0.0, 1.0). The fuzzy inference table is shown in Table 5.

The fuzzy inference process includes the following nine fuzzy rules:

- i. $P_1 = \text{if } S_1 \text{ and } S_2 \text{ then } U \text{ is } VS.$
- ii. $P_2 = \text{if } S_1 \text{ and } M_2 \text{ then } U \text{ is } S.$
- iii. $P_3 = \text{if } S_1 \text{ and } L_2 \text{ then } U \text{ is } M.$
- iv. $P_4 = \text{if } M_1 \text{ and } S_2 \text{ then } U \text{ is } S.$
- v. $P_5 = \text{if } M_1 \text{ and } M_2 \text{ then } U \text{ is } M.$
- vi. $P_6 = \text{if } M_1 \text{ and } L_2 \text{ then } U \text{ is } L.$
- vii. $P_7 = \text{if } L_1 \text{ and } S_2 \text{ then } U \text{ is } M.$
- viii. $P_8 = \text{if } L_1 \text{ and } M_2 \text{ then } U \text{ is } L.$
- ix. $P_9 = \text{if } L_1 \text{ and } L_2 \text{ then } U \text{ is } VL.$

For the final defuzzification process, the weighted average method is used to obtain the final output:

$$P^* = \frac{\sum_i P(P_i) \times P_i}{\sum_i P_i}, \quad (3)$$

where P_i is the weighting coefficient, $P(P_i)$ is the membership degree, and P^* is the final output.

The final obtained MPCI values obtained after the inference process are listed in Table 6.

3.4 Derivation of dual response surface model

The average value of the MPCI values for the four central-point experiments is calculated as

$$\bar{y}_C = (0.4871 + 0.4412 + 0.4798 + 0.4153) / 4 = 0.4559. \quad (4)$$

The average value of the MPCI values for the sixteen experimental runs is calculated as

$$\bar{y}_F = \left(\begin{array}{l} 0.5166 + 0.6936 + 0.5019 + 0.6046 + 0.4556 + 0.5428 \\ + 0.4261 + 0.5184 + 0.5449 + 0.8076 + 0.5033 + 0.5264 \\ + 0.4878 + 0.6986 + 0.4510 + 0.3838 \end{array} \right) / 16 = 0.5414. \quad (5)$$

Table 6
MPCI values for the 16 experimental runs and four central-point experiments.

| Measuring precision | Measuring time | MPCI value |
|---------------------|----------------|------------|
| 357.1429 | 0.01293 | 0.5166 |
| 454.5455 | 0.01358 | 0.6936 |
| 322.5806 | 0.01379 | 0.5019 |
| 384.6154 | 0.01363 | 0.6046 |
| 303.0303 | 0.01365 | 0.4556 |
| 370.3704 | 0.01352 | 0.5428 |
| 250.0000 | 0.01385 | 0.4261 |
| 344.8276 | 0.01367 | 0.5184 |
| 344.8276 | 0.01384 | 0.5449 |
| 454.5455 | 0.01451 | 0.8076 |
| 357.1429 | 0.01345 | 0.5033 |
| 416.6667 | 0.01308 | 0.5264 |
| 270.2703 | 0.01416 | 0.4878 |
| 400.0000 | 0.01399 | 0.6986 |
| 250.0000 | 0.01401 | 0.4510 |
| 303.0303 | 0.01339 | 0.3838 |
| 312.5000 | 0.01377 | 0.4871 |
| 294.1176 | 0.01364 | 0.4412 |
| 333.3333 | 0.01357 | 0.4798 |
| 312.5000 | 0.01388 | 0.4153 |

The sum of the curvature variances is expressed as

$$SS_C = \frac{n_F n_C (\bar{y}_F - \bar{y}_C)^2}{n_F + n_C} = \frac{16 \times 4 (0.5414 - 0.4559)^2}{16 + 4} = 0.02339. \quad (6)$$

The sum of the error variances is expressed as

$$SS_E = \sum_{i=1}^{n_C} (y_i - \bar{y}_C)^2 = 0.0034. \quad (7)$$

The F-statistics value is

$$F = \frac{SS_C / 1}{SS_E / (n_C - 1)} = \frac{0.02339}{0.0034 / (4 - 1)} = 20.58567. \quad (8)$$

After performing regressive analysis for the 20 experimental runs, a regressive model is obtained. Since the curvature is small, the first-order statistical model is selected to approximate the studied problem.

The average response surface is expressed as

$$\begin{aligned} E_Z(y(x, z)) &= b_0 + x'b + x'Bx \\ &= Q_1 + Q_2x_1 + Q_3x_2 + Q_4x_3 \\ &\quad + Q_7x_1x_2 + Q_8x_1x_3 + Q_9x_2x_3 \\ &= 0.524320 + 0.055538x_1 - 0.052000x_2 - 0.045925x_3 \\ &\quad - 0.036675x_1x_2 - 0.015150x_1x_3 + 0.001312x_2x_3. \end{aligned} \quad (9)$$

The average response surface is shown in Fig. 16 and the contour plot is shown in Fig. 17. Two essential variables are selected to plot the 3D response surface. Fixing $x_2 = -1.0$, x_1 and x_3 are selected to plot the 3D response surface.

The variance response surface is defined as

$$Var_Z(y(x, z)) = \sum (\partial y / \partial z_i)^2 \sigma_{z_i}^2 = (\partial y / \partial z_1)^2 \sigma_{z_1}^2 + (\partial y / \partial z_2)^2 \sigma_{z_2}^2. \quad (10)$$

The two partial derivative terms in Eq. (10) are calculated as

$$\partial y / \partial z_1 = -0.001862x_1 - 0.032300x_2 + 0.000800x_3 + 0.008988, \quad (11)$$

$$\partial y / \partial z_2 = -0.004912x_1 - 0.002625x_2 - 0.028025x_3 - 0.007363. \quad (12)$$

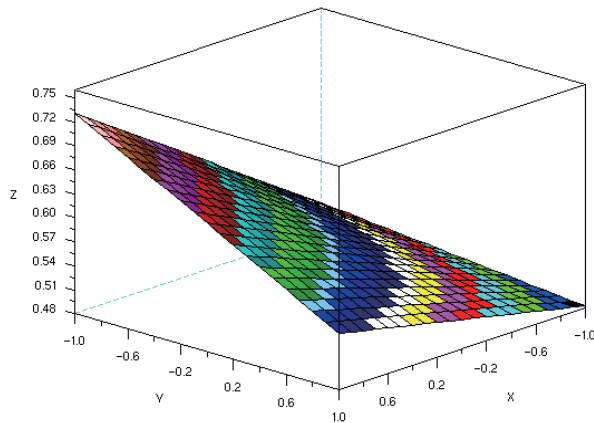


Fig. 16. (Color online) Three-dimensional plot of average response surface.

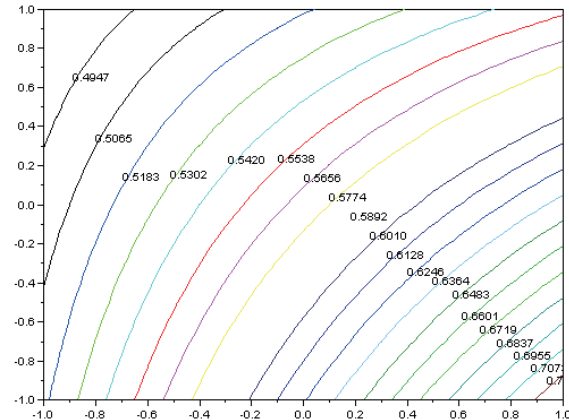


Fig. 17. (Color online) Contour plot of average response surface.

Assuming that the standard deviation is 1.0 for noise factors z_1 and z_2 , the variance response surface is further expressed as

$$\begin{aligned} \text{Var}_z(y(x, z)) = & 0.0001350 + 0.0000389x_1 - 0.0005419x_2 + 0.0004270x_3 \\ & + 0.0001461x_1x_2 + 0.0002724x_1x_3 + 0.0000955x_2x_3 \\ & + 0.0000276x_1^2 + 0.0010502x_2^2 + 0.0007860x_3^2. \end{aligned} \quad (13)$$

The variance response surface is shown in Fig. 18 and the contour plot is shown in Fig. 19. The variance response surface is converted into a constraint in the optimization problem. The constraint condition is expressed as

$$\begin{aligned} \text{Var}_z(y(x, z)) = & 0.0001350 + 0.0000389x_1 - 0.0005419x_2 + 0.0004270x_3 \\ & + 0.0001461x_1x_2 + 0.0002724x_1x_3 + 0.0000955x_2x_3 \\ & + 0.0000276x_1^2 + 0.0010502x_2^2 + 0.0007860x_3^2 \leq 100, \end{aligned} \quad (14)$$

where the constraints of the three control factors are in the range of $(-1.0, 1.0)$, i.e.,

$$-1 \leq x_1 \leq 1, \quad -1 \leq x_2 \leq 1, \quad -1 \leq x_3 \leq 1. \quad (15)$$

4. Optimal Solution by Orthogonal Particle Swarm Optimization

4.1 Orthogonal particle swarm optimization (OPSO) modeling

We discuss the optimization process used to derive the optimal solution in the studied problem based on the statistical model derived by the RSM. The optimal solution may be located anywhere in the range between -1.0 and $+1.0$ and a local optimal solution may not be the optimal

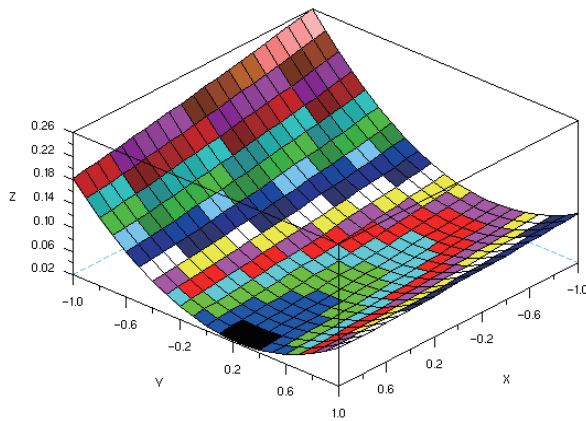


Fig. 18. (Color online) Three-dimensional plot of variance response surface.

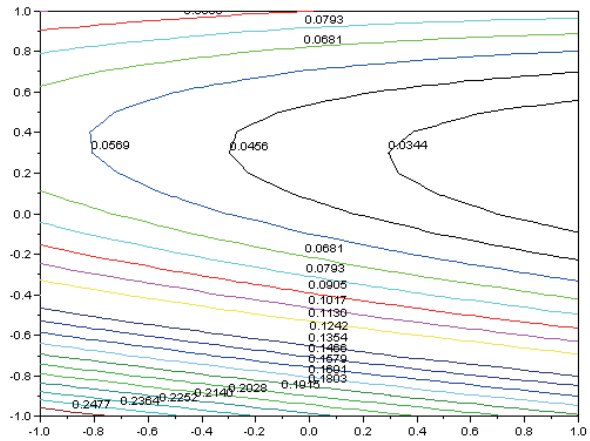


Fig. 19. (Color online) Contour plot of variance response surface.

solution over the entire global range. Therefore, OPSSO is used to efficiently derive the optimal solution. The local and global search processes are combined. The global optimal solution is found during the search for the optimal solution.

If the global solution is more optimal than a local solution, OPSSO can escape from the local optimal solution by adding random seeds into the formulation. In the RSM, the nonlinear problem is approximated as a first-order statistical model problem. However, the curvature of this first-order model is not negligible. Thus, the nonlinearity property is still obvious in this problem. The nonlinearity affects the search process when the algorithm approaches the optimal solution.

Particle swarm optimization (PSO) was derived by emulating the group dynamic behavior of animals.^(18–21) For each particle in a group, not only the individual particle but also the overall group can affect the dynamic behavior. In PSO, position and velocity vectors are defined for each particle. The proposed search method combines the contribution of each individual particle with the contribution of the group. For particles at points in a search space with D dimensions, the i th particle associated with the problem is defined as

$$X_{id} = (r_{i1}, r_{i2}, \dots, r_{iD}), \tag{16}$$

where $d = 1, 2, \dots, D$ and $i = 1, 2, \dots, PS$ with PS the population size. The individual particle value and the group value associated with each particle X_{id} are respectively defined as

$$P_{pd} = (p_{p1}, p_{p2}, \dots, p_{pD}), \tag{17}$$

$$P_{gd} = (p_{g1}, p_{g2}, \dots, p_{gD}). \tag{18}$$

The refreshing speed vector is defined as

$$V_{id} = (v_{i1}, v_{i2}, \dots, v_{iD}). \tag{19}$$

The refreshing position and velocity vectors for step n are expressed as

$$V_{id}^{n+1} = V_{id}^n + c_1 \times rand() \times (P_{pd} - X_{id}^n) + c_2 \times rand() \times (P_{gd} - X_{id}^n), \quad (20)$$

where $X_{id}^{n+1} = X_{id}^n + V_{id}^n$.

The initial estimate of the solution should be made at the start of the search process. In the iteration process, each particle is updated by the values originating from both the group contribution and the individual particle contributions. The convergence condition is the minimum average square error of the particles in the group. The contributions of both the individual particles and the group are mixed together in the searching process.

There may be a local minimum in the optimization problem at which the solution may be trapped, which is not the global minimum solution over the entire range. By considering the group contribution, a random function is adopted to jump out of the local interval. An inertia weighting factor is also introduced in this algorithm to increase the convergence rate. The inertia weighting factor in Eq. (20) and the modified formula are

$$V_{id}^{n+1} = W \times V_{id}^n + c_1 \times rand() \times (P_{pd} - X_{id}^n) + c_2 \times rand() \times (P_{gd} - X_{id}^n), \quad (21)$$

$$W = W_{max} - \frac{W_{max} - W_{min}}{gen_{max}} \times gen, \quad (22)$$

where c_1 and c_2 are both constants, W_{max} is the initial weighting value, W_{min} is the final weighting value, gen is the current generation number, and gen_{max} is the final generation number. However, this modification is actually a linear modification. Many nonlinear modification methods to refresh the velocity vector have been proposed to make such an algorithm suitable for nonlinear search problems. The modified term is defined as the key factor. By setting the learning factors c_1 and c_2 to larger than 4.0, the modification in the speed vector is expressed as

$$V_{id}^{n+1} = K \times [V_{id}^n + c_1 \times rand() \times (P_{pd} - X_{id}^n) + c_2 \times rand() \times (P_{gd} - X_{id}^n)], \quad (23)$$

$$K = \frac{2}{\left| 2 - \left(c_1 + c_2 - \sqrt{(c_1 + c_2)^2 - 4 \times (c_1 + c_2)} \right) \right|}. \quad (24)$$

However, the modified term is rather complicated and not convenient to apply in the search process. In the following, a modified PSO method called orthogonal PSO (OPSO) is proposed to improve the searching process effectively. A simple orthogonal array obtained by the Taguchi method is used in this algorithm to simplify the search process.

4.2 Orthogonal algorithm

In the Taguchi method, two objective functions are defined before performing OPSO. The particle swarms are composed of an individual particle swarm O_{id} and a group swarm A_{id} expressed as follows.

$$O_{id} = X_{id}^n + WV_{id}^n + c_1 \times rand() \times (P_{pd} - X_{id}^n) \tag{25}$$

$$A_{id} = X_{id}^n + WV_{id}^n + c_2 \times rand() \times (P_{gd} - X_{id}^n) \tag{26}$$

The two functions are functions of the three control factors in OPSO. Three levels are defined for the control factors. Therefore, the orthogonal array has three control factors with three levels. We assume that the optimal solution is expressed as Q_{id} , then Q_{id} is adopted to refresh the particle position and velocity vectors using Eqs. (27) and (28). The process for refreshing particles in OPSO is illustrated in Fig. 20.

$$V_{id}^{n+1} = Q_{id} - X_{id}^n \tag{27}$$

$$X_{id}^{n+1} = Q_{id} \tag{28}$$

4.3 Derivation of optimal solution

The optimal solution for the optimization problem was found using the above formulation. The optimal measuring precision and measuring time were found at the same time by the

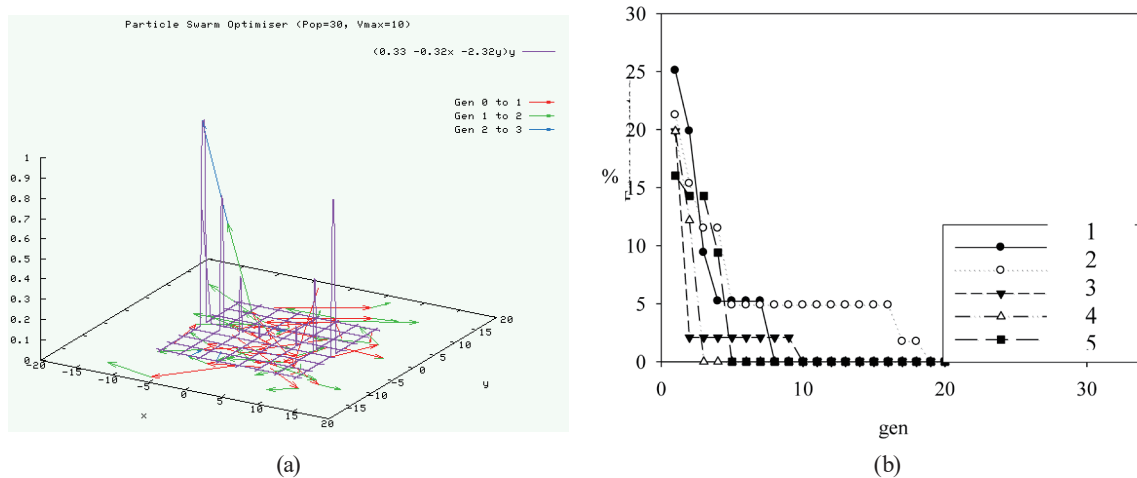


Fig. 20. (Color online) Illustration of OPSO process in the optimization problem. (a) Refreshing process from first generation to third generation. (b) Error percentage from first generation to fifth generation.

proposed MPCl method. The derived optimal solution provided the optimal measuring precision and measuring time for the testing machine.

The statistical model of the studied problem was verified by the RSM and the OPSO method. This model is very applicable for associated smart machinery and industrial applications. The optimal solution can be found at the ends of the entire search range, so that the global solution is found instead of a local solution. Our results showed that the proposed mathematical method can provide a satisfactory search process.

The optimal solution probably lies somewhere between the end points. In OPSO, global and local particles are searched at the same time, resulting in faster convergence than conventional search methods. Related verification experiments showed that the proposed methodology can provide a good prediction. The proposed optimal solution obtained by OPSO can optimize the machine parameters of the measuring precision and measuring time.

In Case 3, the optimal value is obtained as $(x_1, x_2, x_3) = (1.0, -1.0, -1.0)$. This means that the coaxial light should be set to 30%, the four-split ring light should be set to 50%, and the mask position should be set to 10% of the distance moved in the z-direction. The practical optimal value of measuring precision is 0.00619 mm and the practical optimal value of measuring time is 68.64 s.

5. Discussion

We discuss our results by comparing three testing results with different objective functions. As listed in Table 7, Cases 1–3 are compared, where the cases are defined in Sect. 3.2.

Since the curvature of Cases 1–3 is sufficiently small, a first-order statistical model is used to approximate the problem under study. The measuring time of 68.64 s in Case 3 is slightly smaller than the value of 69.31 s in Case 2. The measuring precision of 0.00619 mm in Case 3 is similar to that of 0.00624 mm in Case 1. Satisfactory results were obtained for the studied problem.

Table 7
Comparison of Cases 1–3.

| | Case 1 Measuring precision | Case 2 Measuring time | Case 3 Measuring precision and measuring time | |
|---|-------------------------------|--------------------------|---|----------------------|
| Analytic method | Response surface method | Response surface method | Fuzzy inference response surface method | |
| Objective function | Nominal-the-best | Smaller-the-better | Nominal-the-best and smaller-the-better | |
| Optimal solution | (1.0, -1.0, -1.0) | (1.0, -1.0, -1.0) | (1.0, -1.0, -1.0) | |
| Curvature | 16.0234 | 20.62051 | 20.58567 | |
| Maximal testing set in combinational table | 454.5455 (0.0062 mm) | 0.01451 (68.92 s) | 455.5455 (0.00619 mm) | 0.01457 (68.64 s) |
| Optimal value | 445.10 (0.00624 mm) | 0.01443 (69.31 s) | 455.5455 (0.00619 mm) | 0.01457 (68.64 s) |

6. Conclusion

With the decreasing size of electronic components and the increasing integration of chipsets, higher measuring precision is required to inspect defects. By studying the optimal lighting system, the image sensing effect and measuring precision can be enhanced to inspect workpiece defects. Also, the measuring time is studied to obtain the shortest measuring time and thus increase the generation efficiency. Control factors related to the negative lighting system such as a backlighting system can also be added to assess the improvement of the measuring precision and measuring time in the future.

It is expected that the proposed statistical method can be applied in a website server and uploaded onto a cloud server. Smart manufacturing and intelligent sensing and inspection processes can be achieved to increase generation efficiency in the era of Industry 4.0.

Acknowledgments

The experimental setup employed in this study was partially supported by Tzan-Hsing Inc.

References

- 1 K. J. Stout: Three Dimensional Surface Topography: Measurement, Interpretation and Application (Penton Press, Cleveland, 1994).
- 2 P. V. C. Hough: Methods and Means for Recognising Complex Patterns, U.S. patent 3069654 (1962).
- 3 H. Cao: *J. Measurement* **31** (2002) 71.
- 4 T. G. Beckwith and R. D. Marangoni: *Mech. Measurements* (Addison-Wesley, Boston, 2003).
- 5 K. Kawasue and T. Ishimatsu: *IEEE Trans. Ind. Electron.* **44** (1997) 703.
- 6 M. Subbarao and T. Choi: *IEEE Trans. Pattern Anal. Mach. Intell.* **17** (1995) 266.
- 7 A. P. Pentland: *IEEE Trans. Pattern Anal. Mach. Intell.* **9** (1987) 523.
- 8 S. K. Nayar and Y. Nakagawa: *Proc. Int. Conf. Robotics and Automation* (1990) 218–225.
- 9 S. K. Nayar and Y. Nakagawa: *IEEE Trans. Pattern Anal. Mach. Intell.* **16** (1994) 824.
- 10 D. Lu and J. Antony: *Intl. J. Prod. Res.* **40** (2002) 1613.
- 11 Y. S. Tarn, W. H. Yang, and S. C. Juang: *Int. J. Adv. Manuf. Technol.* **16** (2000) 688.
- 12 L. I. Tong, C. H. Wang, and H. C. Chen: *Int. J. Adv. Manuf. Technol.* **27** (2005) 407.
- 13 F. C. Wu: *J. Manuf. Syst.* **23** (2004) 134.
- 14 R. H. Myers and D. C. Douglas: *Response Surface Methodology: Process and Product Optimization Using Designed Experiments* (Wiley, New York, 1995).
- 15 K. Koyamada, K. Sakai, and T. Itoh: *Proc. Annu. Int. Conf. IEEE EMBS, IEEE* (2004) 2909–2912.
- 16 A. Parkinson: *Trans. ASME* **117** (1995) 48.
- 17 S. Sundaresan, K. Ishii, and D. R. Houser: *Proc. ASME Advance in Design Automation Conf., ASME* (1993) 379–386.
- 18 Y. Shi and R. Eberhart: *Proc. IEEE Int. Conf. Evolutionary Computation, IEEE* (1998) 69–72.
- 19 R. Eberhart and Y. Shi: *Proc. Congr. Evolutionary Computation* (2000) 84–88.
- 20 S. Y. Ho: *IEEE Trans. Syst. Man Cybern.* **38** (2008) 288.
- 21 B. Y. Qu, P. N. Suganthan, and S. Das: *IEEE Trans. Evol. Comput.* **17** (2013) 387.